Atomistic Simulation of Nickel Surface and Interface Properties

Anika Marusczyk, Senja Ramakers, Matthias Kappeler, Patricia Haremski, Matthias Wieler, and Piero Lupetin

Abstract This report describes the research conducted by use of the ForHLRI within the publicly funded project 'Kersolife100', in which the long-term performance of a fully ceramic solid oxide fuel cell (SOFC) concept is investigated. The project aims at modeling and understanding the dominant degradation mechanisms in SOFCs so that the required lifetime of the SOFC-stacks can be ensured. One major cause of ageing is the unfavourable microstructural evolution of the nickel-based anode that occurs upon SOFC operation. The associated mechanisms are modeled by use of phase field methods within 'Kersolife100'. For a successful outcome, the availability of accurate material parameters is crucial, but until now not given. Complementary to experimental efforts, the ab-initio research activities of this year therefore focused on the determination of the relevant nickel surface and interface properties. By combining experimental and simulation results, a deeper understanding of the anode aging mechanism can be generated and the identification of counter measures can be guided. In this report, the current results of the ab-initio activities are summarized.

1 Compuational Methods

In this work, all density functional theory calculations were performed with the Vienna Ab initio Simulation Package (VASP, version 5.4.1 on ForHLR I) [14–17] using the Projector Augmented Wave Method (PAW) [1, 18] while treating the nickel p-states as valence states. During structural optimization, the Methfessel-Paxton smearing method with $\sigma=0.01$ was used to determine the partial orbital occupancies. To obtain highly converged results, a static energy calculation using the tetrahedron method with Bloechl correction was then conducted. The slab and grain boundary structures were constructed from fully relaxed bulk structures including spin-polarization and only ionic relaxation was allowed for the total energy calculation of the slabs. The convergence criterion was held constant for all calculations

A. Marusczyk (✉) · S. Ramakers · M. Kappeler · P. Haremski · M. Wieler · P. Lupetin
Corporate Sector Research and Advance Engineering, Rober Bosch GmbH,
Robert-Bosch-Campus 1, 71272 Renningen, Germany
e-mail: Anika.Marusczyk@de.bosch.com

at 10^{-8} eV for the electronic cycle and 10^{-6} eV for the ionic cycle. To achieve highly accurate results, careful convergence analyses regarding cell size, relaxation methods, exchange-correlation functional, plane-wave cutoff and gamma-centered k-mesh were conducted, the results of which will be described in the following sections. For the job management, the Automated Interactive Infrastructure and Database for Computational Science (AiiDa) [30] software was used in combination with Custodian [26]. The crystal structures were generated with the Atomic Simulation Environment (ASE) [19] as well as the Python Materials Genomics (pymatgen) [26] and Vesta [25] was used for the visualization. The empirical potential calculations were performed with enlarged (2×2 and 3×3) cells using LAMMPS [31] with a convergence criterion of $\epsilon = 10^{-4}$ eV.

2 Nickel Surface Energies and Anisotropies

Nickel surface energies and anisotropies are of crucial importance as input parameters for the phase field simulations as they are likely to play a dominant role in the microstructural evolution of the Ni-based anode upon SOFC operation. At the same time, their experimental determination is highly challenging and the expected scatter due to the measurement methods is significant (compare e.g. Refs. [2, 5, 20, 32, 37, 40, 41]). At the same time, the determination of accurate metallic surface energies with ab-initio methods is highly non-trivial and careful convergence as well as exchange-correlation functional evaluations were conducted to obtain reliable energy values. The computational details of our efforts to determine these energies will be described in the next sections.

2.1 Convergence Parameters and Technical Details

The surface energy γ is defined as the difference between the energy of the surface structure E_{surf} and the bulk structure E_{bulk} normalized to the area of the surface A [40]:

$$\gamma = \frac{1}{2A}(E_{\text{surf}} - N \cdot E_{\text{bulk}}). \tag{1}$$

To determine E_{surf}, the slab method was used and the surface was modeled as a perfect fcc nickel phase with two interfaces to the vacuum due to the periodic boundary conditions. As a consequence, additional convergence parameters to the plane-wave cutoff and the k-mesh were considered for the slab calculations. These include the size of the vacuum and the number of atomic layers in the slab to ensure minimal interaction between the two surfaces, as well as the number of layers to be relaxed upon each optimization to account for the deceased tight binding of surface atoms
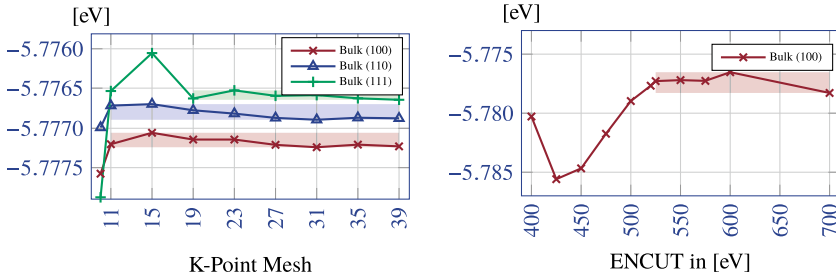
Fig. 1 Convergence of the total energy of bulk Ni fcc with respect to the k-mesh (left) and plane-wave cutoff (right)
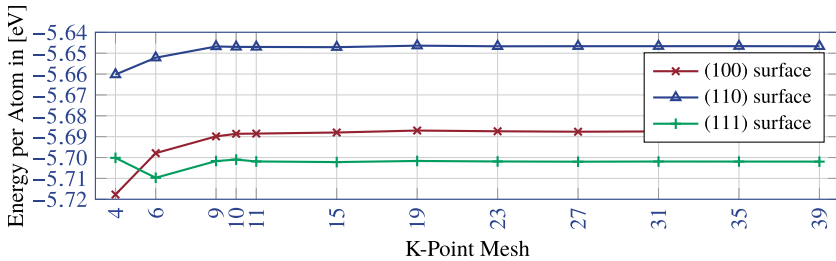

Fig. 2 Convergence of the total energy with respect to the vacuum size for low Miller index orientations of the surface

compared to those in the bulk. We calculated the ground state energies of differently oriented surfaces characterized by their Miller indices and to achieve high accuracy, the bulk energies E_{bulk} for low Miller index ($<=1$) structures were calculated for the corresponding orientations of the bulk as well.

Convergence analyses were conducted for the three chosen exchange-correlation functionals (local density approximation (LDA) [4], generalized gradient approximation under the Perdew-Burker-Ernzerhof parametrization (PBE) [27, 28], generalized gradient approximation for solids and surfaces (PBEsol) [29]) and representative results for the plane-wave cutoff and the k-mesh are depicted in Fig. 1. These fast calculations for the small bulk structures were used as a guideline for the convergence evaluation of the computationally more demanding slab structures. Representative results for the low Miller index orientation surfaces with respect to the the vacuum slab, number of relaxed layers and slab size can be found in Figs. 2, 3 and 4. Based on these calculations, we chose a k-mesh of $23 \times 23x1$, a plane-wave cutoff of 550 eV, a vacuum slab of 14 $\mathring{A}$, a cell size of 13–17 layers and relaxed 2–4 layers.
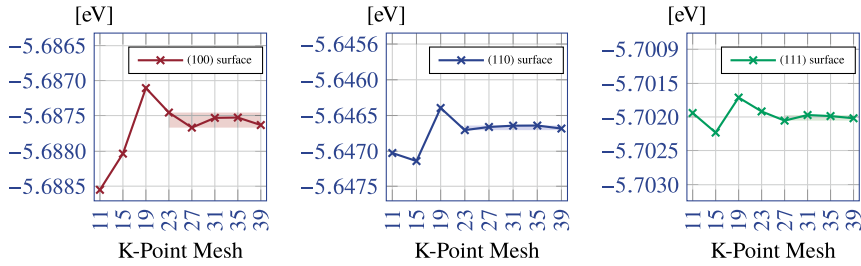
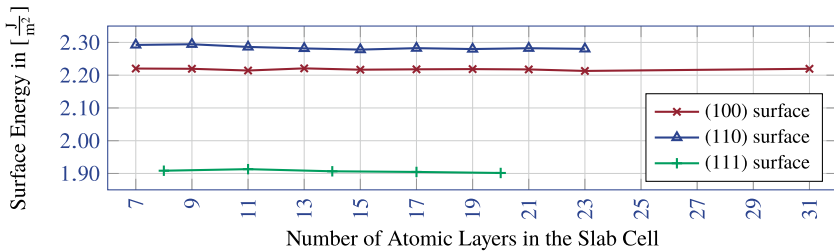**Fig. 3** Convergence of the total energy with respect to the number of relaxed layers

Fig. 4 Convergence of the surface energy with respect of the total atomic layers in the slab

2.2 Surface Energies

The results of our surface energy calculations have been submitted to Acta Materialia and are described in detail in the corresponding article. The surface energies, γ_{hkl}, for low Miller index structures were determined with the three exchange-correlation functionals, all of which lead to excellent agreement within the expected experimental scatter. However, LDA is known to overestimate [3] and GGA-PBE to underestimate surface energies [42] while the GGA-PBEsol value, which was in between the other two, is expected to be most reliable. It was therefore used for the calculation of structures with higher Miller indices.

To obtain these results, calculations on 80 or 120 CPUs (depending on the cell size) with an average runtime of 18h were conducted. Surfaces with higher Miller index orientations require larger unit cells and therefore the average runtime on 120 CPUs amounted to 140 h. Due to the requirement of high accuracy, we chose strict numerical parameters and cutoffs for our calculations. This led to frequent convergence issues, especially for larger cell sizes, that were solved by increasing the number of cores and runtime. It should be noted that the parallelization of VASP can be controlled by defining the number of bands that are treated in parallel (NPAR-tag). We made use of this option for the slab calculations, requiring at least 80 CPUs, and fixed the parameter to 8, as recommended by the VASP manual (NPAR $\approx \sqrt{\text{\#cores}}$).

Clearly, the calculation of accurate surface energies using ab-initio methods is computationally very demanding. Empirical potentials constitute a much less expen-

Table 1 Empirical potentials and their abbreviations used in this work

Abbreviation	Potential	Source
EAM_fcc	Embedded-atom-method functions for the fcc metals	[10, 11]
EAM_TCS	EAM Angelo Moody Baskes modified by Tehranchi Curtin Song	[8, 9, 38, 39]
EAM_DMF	EAM Dynamo Mishin Farkas	[23, 24]
EAM_DM	EAM Dynamo Mendelev	[21, 22]
Pair_Morse	Pair Morse Shifted GirifalcoWeizer HighCutoff	[6, 7, 12]
EMT	EMT Asap Standard Jacobsen Stoltze Norskov	[13, 35, 36]

sive method and if they provided reliable results, their use would therefore be highly desirable. To investigate this issue, we benchmarked a set of six available empirical potentials (Table 1) from the OpenKim database [38] and compared them to our accurate density functional theory values. The chosen potentials differ in their model or fitting method. While the embedded atom method potential EAM_fcc has been fitted to the sublimation energy, equilibrium lattice constant, elastic constants, vacancy-formation energies of the pure metals and the heat of solution of the binary alloys, EAM_DMF has been fitted to experimental and ab initio data for monoatomic nickel and EAM_DM to liquid and gas properties. Pair_Morse is a Pair Morse potential fitted to the energy of vaporization, the lattice constant and the compressibility and EMT is an Effective Medium Theory potential fitted to bonding in metallic systems. EAM_TCS is the only embedded atom method potential that also includes an interaction between Ni and H.

We found EAM_TCS to give the most reliable weighted surface energies within 10 % accuracy. However, none of the used empirical potentials correctly reproduced the energetic hierarchy determined by density functional theory. In view of first phase field simulations conducted at the Hochschule Karlsruhe that revealed the importance of anisotropy to correctly describe the microstructural evolution of the Ni-based anode, the observed discrepancy in predicting the relative energies between the accurate PBEsol and empirical potential method prohibits the use of latter for our purposes. While we will still refer to empirical potentials in future work packages whenever possible, density functional theory calculations will continue to be the focus of this project. For this work package, direct calculation on the visualization nodes was feasible.

3 Nickel Grain Boundary Energies

Nickel grain boundary energies are important material parameters to be used as input for the phase field simulations and their determination constitutes an ongoing work package. The grain boundary energy γ_{GB} is calculated as the difference in energy between structures with and without a grain boundary

$$\gamma_{GB} = \frac{E_{GB,tot} - N \cdot E_{bulk}}{2A_{GB}}, \tag{2}$$

where $E_{GB,tot}$ is the total energy of the system with two grain boundaries due to periodic boundary conditions, N is the number of atoms in the system, E_{bulk} the energy of the bulk per atom, and A_{GB} the surface area of the grain boundary.

In a first step, the necessary parameters to achieve high accuracy were evaluated and using our research on nickel surface energies as a guideline, we conducted a reduced convergence analysis regarding the planewave cutoff and k-mesh for a $\Sigma 3(111)60°$ twist boundary that is expected to be highly stable [3]. For further calculations, we chose a k-mesh of $12x\frac{12}{b}x\frac{12}{c}$ ($\approx 3.5\mathring{A}$) and 550 eV as a planewave cutoff, consistent with the surface calculations. The convergence analysis was conducted for a 24-atoms cell, using 16 CPUs with an average runtime of 15 min for low k-mesh and planewave cutoff values and an average of 1.5h for high values.

When determining grain boundary energies with density functional theory, convergence with respect to the cell size needs to be ensured. Due to the periodic boundary conditions, each structure has two grain boundary plains and to achieve high accuracy, their interaction should be minimized by increasing the distance between them. After having confirmed the dominance of the c-lattice parameter, we investigated the energy convergence with respect to c for the stable $\Sigma 3$ grain boundary while varying the relaxation method between full, ionic only and fully static. Full relaxation of the structure was found to be needed for accurate results at feasible cell sizes and convergence was reached at a cell length of 50 $\mathring{A}$, in agreement with similar density functional theory calculations for bcc Tungsten [34]. For larger cell sizes, we increased the number of CPUs to 32 for cells up to 72 atoms (average runtime 5h) and 64 for cells up to 144 atoms (average runtime 25h). To ensure efficient parallelization, we made use of the NCORE-tag available in VASP and chose 8 cores per orbital, as recommended in the VASP-manual. The previously used NPAR-tag can be related to NCORE by NCORE=CPUs/NPAR.

Due to the large number of possible grain boundaries in fcc nickel, we are currently investigating the effect of cell size and relative energies with the less computationally expensive empirical potentials. The results will then be benchmarked to those obtained from highly accurate density functional theory calculations for selected structures, whose choice was based on our previous surface energy calculations as well as literature results. Consequently, we constructed symmetric tilt boundaries around the 110-axis for the four most stable surface orientations as previously determined. Our current results and computational details are shown in Table 2, demonstrating good agreement with values known from the literature [33]. For these highly

Table 2 Grain boundary energy results and computational details of the four most stable grain boundaries

Sigma	# atoms	Plane	Twist	Tilt	γ_{GB} mJ/m^2	CPUh	# CPUs
3	48	111	rot. axis: (111) angle: 60/180	rot. axis: (110) angle: 109.5	58.5	2.36	32
3	20	211	rot. axis: (211) angle: 180	rot. axis: (110) angle: 70.5	1283.1	5.39	32
9	68	221	rot. axis: (221) angle: 180	rot. axis: (110) angle: 141.1	1211.1	29.83	96
11	88	311	rot. axis: (311) angle: 180	rot. axis: (110) angle: 50.5	517.0	9	160

converged calculations, we increased the number of CPUs to 96 for large cells while keeping NCORE at 8. The results generated in this workpackage will be published in a scientific journal.

4 Nickel Surface Self-Diffusion Constants

Based on an internal evaluation of experimental results, nickel surface diffusion is expected to play a dominant role in the microstructural evolution of the anode. It is expected to involve the migration of adsorbed nickel atoms and therefore knowledge of stable nickel adsorption sights on the nickel surfaces, including the atomistic models, is needed in a first step. Our derived results are described in detail in the submitted paper (compare Sect. 2). The relevant energy barriers for the migration of a nickel atom on the surface can then be calculated using the Nudged Elastic Band method (NEB) and by considering differently oriented surfaces, the effect of anisotropy on the diffusion constants can be assessed. In addition to this, the influence of the expectedly adsorbed hydrogen atoms on the diffusion constant should be investigated, which is why we also considered the adsorption of hydrogen on nickel surfaces. It should be noted that the derived diffusion constants should be evaluated in close comparison to available diffusion constant values. Depending on the outcome, an extension or reduction of the methodology (e.g. explicit calculation of vibrational entropies or the use of empirical potentials) should be considered.

The adsorption energies of nickel on the expected stable sites of the low Miller index surfaces were calculated using density functional theory as well as the most promising empirical potential EAM_TCS (compare Table 1). We found an excellent agreement between both methods, which is why the computationally much less expensive empirical potential constitutes an attractive alternative for similar future research questions. Opposed to this, the adsorption of hydrogen on Ni surfaces using empirical potentials did not give reliable results and density functional theory calcu-

lations, predicting a relative stability of hydrogen adsorption sites in agreement with the literature, are indispensable. The derived atomistic models will be used to investigate the influence of hydrogen on the nickel surface self-diffusion constants. The density functional theory calculations were performed on 80 or 120 CPUs depending on the cell size with an average calculation time of 120 h.

In order to determine the desired diffusion constants as input for the phase field simulations, first energy barrier calculations for the simplest case, an interstitial hopping mechanism, were conducted using the Nudged Elastic Band method. In a first step, the thermodynamically stable (111) surface was considered and the minimal energy path was guessed by interpolation. To be feasible, the k-mesh was reduced to $9 \times 5 \times 1$ for a $2 \times 1 \times 1$ supercell and the effect of the number of images as well as the number of fixed atoms was investigated. First calculations led to unconverged results and underestimated energy barriers and the most promising numerical parameters and methods are currently under investigation. The NEB calculations were conducted on 64 or 144 CPUs depending on the number of images with an average runtime of 15–50 h.

5   Summary and Outlook

The goal of this project is the determination of the most relevant material parameters of a Ni-based SOFC anode to be used as input parameters for phase field simulations conducted within the publicly funded project 'Kersolife100'. These strive to model the microstructural evolution of the anode under SOFC operating conditions in order to make understanding driven predictions of its long-term performance. Within the reporting period, our research activities focused on the determination of the relevant nickel surface energies, nickel grain boundary energies and nickel surface self-diffusion constants using density functional theory. After having conducted extensive convergence analyses to obtain highly accurate nickel surface energies, we considered different surface orientations up to a Miller index of 3 and achieved excellent agreement with known literature values within the expected scatter. First phase field simulations revealed the importance of anisotropy for the accurate prediction of the microstructural evolution of the Ni-based anode, excluding the possibility to use the computationally much less demanding empirical potentials that have so far not lead to a satisfactory description of the anisotropy.

Based on our surface results, we were able to obtain first converged nickel grain boundary energies with a reduced set of convergence tests for selected structures. The latter were chosen based on our knowledge of the stable surfaces as well as literature data and will be used for further analysis of the most reliable methodology. This includes the finalization of our preliminary investigation of cell size convergence and a comparison of our accurate density functional theory results with those derived from the computationally much less demanding empirical potentials. Using the latter, we aim to generate an enhanced understanding of the cell size influence, which is not feasible with density functional theory due to cell size limitations. In addition to

this, we can obtain a qualitative understanding of the relative stability of the immense number of possible grain boundary structures based on which we will perform highly accurate density functional theory calculations for selected structures to be used as input for phase field simulations.

Once pure nickel grain boundaries have been satisfactorily described, the more complicated nickel-electrolyte grain boundaries can be considered. In a first step, the atomistic models for the electrolyte, an Y-stabilized Zr-oxide, must be developed and a reliable description of the bulk oxide must be ensured. The mixed grain boundaries will then be constructed based on our knowledge of pure surfaces and grain boundaries and their determined energies will be transferred to the phase field simulation. Since the mixed structures are expected to become extremely large, it might be necessary to decrease our strict numerical parameters and rely on less accurate results. Since there is currently no data available on mixed nickel-YSZ grain boundaries, this is still expected to be a highly valuable result.

In addition to interfacial energies, diffusion constants are another important input parameter for the phase field simulations. In a first step, we considered nickel surface self-diffusion, which is expected to play a dominant role based on an internal evaluation of experimental results. Since we expect the migration of adsorbed nickel atoms on the surface to be of crucial importance, we determined the stable adsorption sites of nickel on differently oriented stable nickel surfaces and derived the corresponding atomistic models. In addition to this, we also considered the adsorption of hydrogen on the surface in order to investigate its effect on the diffusion constant. Using the derived atomistic models, we conducted first Nudged Elastic Band calculations to determine the relevant energy barriers. Further research is, however, needed to obtain reliable results, which will be part of this year's activities. It should be noted that the derived diffusion constants will be evaluated in close comparison to available experimental values. Depending on the outcome, an extension or reduction of the methodology (e.g.. explicit calculation of vibrational entropies or use of empirical potentials) should be considered. In view of expected timing and resources, grain boundary diffusion constants will likely not be considered within this project.

References

1. P.E. Blöchl, Projector augmented-wave method. Phys. Rev. B **50**, 17953–17979 (1994)
2. E.A. Clark, R. Yeske, H.K. Birnbaum, The effect of hydrogen on the surface energy of nickel. Metall. Trans. A **11**(11), 1903–1908 (1980)
3. G.I. Csonka, J.P. Perdew, A. Ruzsinszky, P.H.T. Philipsen, S. Lebègue, J. Paier, O.A. Vydrov, J.G. Ángyán, Assessing the performance of recent density functionals for bulk solids. Phys. Rev. B **79**, 155107 (2009)

4. S. De Waele, K. Lejaeghere, M. Sluydts, S. Cottenier, Error estimates for density-functional theory predictions of surface energy and work function. Phys. Rev. B **94**, 235418 (2016)

5. R. Digilov, S. Zadumkin, V. Kumykov, K. Khokonov, Measurement of surface tension of refractory metals in solid state. Fiz. Met. Metalloved. **41**, 979–982 (1976)

6. R.S. Elliott, This is a model driver for the morse pair potential shifted to zero energy at cutoff separation (2014), Online Accessed 07 Sept 2018

7. R.S. Elliott, This is a Ni morse model parameterization by girifalco and weizer using a high accuracy cutoff distance (2014) Online Accessed 07 Sept 2018

8. R.S. Elliott, EAM model driver with hermite cubic spline interpolation (2018) Online Accessed 28 Aug 2018

9. R.S. Elliott, E.B. Tadmor, Knowledgebase of interatomic models application programming interface (2011) Online; Accessed 28 Aug 2018

10. S.M. Foiles, M.I. Baskes, M.S. Daw, Embedded-atom-method functions for the fcc metals Cu, Ag, Au, Ni, Pd, Pt, and their alloys. Phys. Rev. B **33**, 7983–7991 (1986)

11. S.M. Foiles, M.I. Baskes, M.S. Daw, Erratum: Embedded-atom-method functions for the fcc metals Cu, Ag, Au, Ni, Pd, Pt, and their alloys. Phys. Rev. B **37**, 10378–10378 (1988)

12. L.A. Girifalco, V.G. Weizer, Application of the Morse potential function to cubic metals. Phys. Rev. **114**, 687–690 (1959)

13. K.W. Jacobsen, P. Stoltze, J.K. Nørskov, A semi-empirical effective medium theory for metals and alloys. Surf. Sci. **366**(2), 394–402 (1996)

14. G. Kresse, J. Furthmüller, Efficient iterative schemes for ab initio total-energy calculations using a plane-wave basis set. Phys. Rev. B **54**, 11169–11186 (1996)

15. G. Kresse, J. Furthmller, Efficiency of ab-initio total energy calculations for metals and semiconductors using a plane-wave basis set. Comput. Mater. Sci. **6**(1), 15–50 (1996)

16. G. Kresse, J. Hafner, Ab initio molecular dynamics for liquid metals. Phys. Rev. B **47**, 558–561 (1993)

17. G. Kresse, J. Hafner, Ab initio molecular-dynamics simulation of the liquid-metal-amorphous-semiconductor transition in germanium. Phys. Rev. B **49**, 14251–14269 (1994)

18. G. Kresse, D. Joubert, From ultrasoft pseudopotentials to the projector augmented-wave method. Phys. Rev. B **59**, 1758–1775 (1999)

19. A.H. Larsen, J.J. Mortensen, J. Blomqvist, I.E. Castelli, R. Christensen, M. DuAĆak, J. Friis, M.N. Groves, B. Hammer, C. Hargus, E.D. Hermes, P.C. Jennings, P.B. Jensen, J. Kermode, J.R. Kitchin, E.L. Kolsbjerg, J. Kubal, K. Kaasbjerg, S. Lysgaard, J.B. Maronsson, T. Maxson, T. Olsen, L. Pastewka, A. Peterson, C. Rostgaard, J. Schiotz, O. Schaijtt, M. Strange, K.S. Thygesen, T. Vegge, L. Vilhelmsen, M. Walter, Z. Zeng, K.W. Jacobsen, The atomic simulation environment—a python library for working with atoms. J. Phys.: Condens. Matter **29**(27), 273002 (2017)

20. P.S. Maiya, J.M. Blakely, Surface self a diffusion and surface energy of nickel. J. Appl. Phys. **38**(2), 698–704 (1967)

21. M. Mendelev, M. Kramer, S. Hao, K. Ho, C. Wang, Development of interatomic potentials appropriate for simulation of liquid and glass properties of NiZr2 alloy. Phil. Mag. **92**(35), 4454–4469 (2012)

22. M.I. Mendelev, Finnis-Sinclair potential for the Ni-Zr system developed by Mendelev et al. (2012) (2018) Online; Accessed 07 Sept2018

23. Y. Mishin, EAM Ni potential (2018) Online; Accessed 07 Sept 2018

24. Y. Mishin, D. Farkas, M.J. Mehl, D.A. Papaconstantopoulos, Interatomic potentials for monoatomic metals from experimental data and ab initio calculations. Phys. Rev. B **59**, 3393–3407 (1999)

25. K. Momma, F. Izumi, VESTA3 for three-dimensional visualization of crystal, volumetric and morphology data. J. Appl. Crystallogr. **44**(6), 1272–1276 (2011)

26. S.P. Ong, W.D. Richards, A. Jain, G. Hautier, M. Kocher, S. Cholia, D. Gunter, V.L. Chevrier, K.A. Persson, G. Ceder, Python materials genomics (pymatgen): A robust, open-source python library for materials analysis. Comput. Mater. Sci. **68**, 314–319 (2013)

27. J.P. Perdew, K. Burke, M. Ernzerhof, Generalized Gradient Approximation Made Simple. Phys. Rev. Lett. **77**(18), 3865–3868 (1996)
28. J.P. Perdew, K. Burke, M. Ernzerhof, Generalized Gradient approximation made simple [Phys. Rev. Lett. 77, 3865 (1996)]. Phys. Rev. Lett. **78**(7), 1396–1396 (1997)
29. J.P. Perdew, A. Ruzsinszky, G.I. Csonka, O.A. Vydrov, G.E. Scuseria, L.A. Constantin, X. Zhou, K. Burke, Restoring the density-gradient expansion for exchange in solids and surfaces. Phys. Rev. Lett. **100**, 136406 (2008)
30. G. Pizzi, A. Cepellotti, R. Sabatini, N. Marzari, B. Kozinsky, Aiida: automated interactive infrastructure and database for computational science. Comput. Mater. Sci. **111**, 218–230 (2016)
31. S. Plimpton, Fast parallel algorithms for short-range molecular dynamics. J. Comput. Phys. **117**(1), 1–19 (1995)
32. T. Roth, The surface and grain boundary energies of iron, cobalt and nickel. Mater. Sci. Eng. **18**(2), 183–192 (1975)
33. M.D. Sangid, H. Sehitoglu, H.J. Maier, T. Niendorf, Grain boundary characterization and energetics of superalloys. Mater. Sci. Eng., A **527**(26), 7115–7125 (2010)
34. D. Scheiber, R. Pippan, P. Puschnig, L. Romaner, Ab initiocalculations of grain boundaries in bcc metals. Modell. Simul. Mater. Sci. Eng. **24**(3), 035013 (2016)
35. J. Schiotz, Effective medium theory as implemented in the ase/asap code (2015). Online; Accessed 07 Sept 2018
36. J. Schiotz, Standard effective medium theory potential for face-centered cubic metals as implemented in ase/asap (2015) Online; Accessed 07 Sept 2018
37. D.R. Stickle, J.P. Hirth, G. Meyrick, R. Speiser, A new technique for measuring the effects of oxygen activity on surface energies: Application to nickel. Metall. Trans. A **7**(1), 71–74 (1976)
38. E.B. Tadmor, R.S. Elliott, J.P. Sethna, R.E. Miller, C.A. Becker, The potential of atomistic simulations and the Knowledgebase of Interatomic Models. JOM **63**(7), 17–77 (2011)
39. A. Tehranchi, A modification of the angelo et al. ni-h potential which enhances the binding energies of h atoms to the gbs in nickel (2018) Online; Accessed 28 Aug 2018
40. R. Tran, Z. Xu, B. Radhakrishnan, D. Winston, W. Sun, K.A. Persson, S.P. Ong, Surface energies of elemental crystals. Sci. Data **3** (2016)
41. W. Tyson, W. Miller, Surface free energies of solid metals: Estimation from liquid surface tension measurements. Surf. Sci. **62**(1), 267–276 (1977)
42. L. Vitos, A. Ruban, H. Skriver, J. Kollar, The surface energy of metals. Surf. Sci. **411**(1), 186–202 (1998)